J Sol-Gel Sci Technol
DOI 10.1007/s10971-007-1655-2

ORIGINAL PAPER

Structural evolution from the sol to the $PbZrO_3$ precursor powders prepared by an alkoxide-based sol–gel route

E. D. Ion · B. Malič · I. Arčon · A. Kodre · M. Kosec

Received: 23 August 2007 / Accepted: 5 November 2007

Abstract $PbZrO_3$ powders have been prepared by an alkoxide-based sol–gel route, starting from lead acetate, zirconium *n*-butoxide, and *n*-butanol as a solvent, and hydrolysed with different amounts of water in neutral and alkaline medium. The local environment of Zr and Pb atoms was pursued from the sol to the dried (150 °C) and heated (400 °C) powders, by extended x-ray absorption fine structure (EXAFS). The analysis of the sol revealed links between Pb and Zr, and even more links between Zr and Zr. The metal neighbourhoods in the dried powders are not influenced by the hydrolysis conditions. Pb-Zr correlations are gradually lost from the sol to the dried and heated powders, while the loss of Zr–Zr correlations is considerably lower.

Keywords $PbZrO_3$ · Alkoxide-based sol–gel · EXAFS

1 Introduction

Lead zirconate titanate ceramics, $Pb(Zr,Ti)O_3$ (PZT) have found a widespread use due to their piezoelectric and ferroelectric properties [1]. One of the methods to prepare PZT powder is the alkoxide-based sol–gel synthesis, by which M–O–M bridges, the building blocks of the oxide network, are established through reactions of hydrolysis and condensation [2].

Lakeman et.al. [3] observed that one of the frequently cited advantages of sol–gel processing was the improved chemical homogeneity that might be achieved in solution. By transmission electron microscopy study, the authors demonstrated that when heated at 300 °C $Pb(Zr_{0.53}Ti_{0.47})O_3$ thin films were compositionally heterogeneous on the nanoscale, and that during heat treatment at 600 °C, through diffusion processes a compositionally uniform perovskite phase resulted. Sengupta et al. [4] found that Pb cations do not participate in the bonding with Ti and Zr in $PbTiO_3$ and PZT amorphous powder heated at 375 °C and 425 °C, respectively; even in the $PbZrO_3$ (PZ) amorphous powder (500 °C) where Zr–O–Pb bonds do form, Zr–O–Zr bonds are still present. Feth et al. [5] found that the local order of metal atoms in the amorphous $PbTiO_3$, PZ, and PZT was completely different from that in the perovskite structure, but resembled the local order of the individual metal oxides: local environment of lead in amorphous samples corresponded to the structure of tetragonal PbO; the local structure around zirconium was similar to that in monoclinic ZrO_2, while Ti environment corresponded to the structure of tetragonal TiO_2. Also, a preferred Zr homo-condensation in the amorphous precursor powder [6] or the 2-methoxyethanol based sol [7, 8] of PZT with a high Zr content was found by Malic et al. For the case of the sol they proposed that during reflux and distillation polynuclear oxo-alkoxide complexes formed by ether elimination.

There are several pathways for formation of the polynuclear oxo-alkoxide complexes, including hydrolysis and condensation as well as non-hydrolytic processes of ether

E. D. Ion (✉) · B. Malič · I. Arčon · A. Kodre · M. Kosec
Jožef Stefan Institute, Jamova 39, Ljubljana 1000, Slovenia
e-mail: elena.ion@ijs.si

E. D. Ion
National Institute of Materials Physics, P.O. Box MG-7, Bucharest-Magurele, Romania

I. Arčon
University of Nova Gorica, Vipavska 13, Nova Gorica 5000, Slovenia

A. Kodre
Faculty of Mathematics and Physics, University of Ljubljana, Jadranska 19, Ljubljana 1000, Slovenia

elimination and desolvation of alcohol. $Ti_{12}O_{16}(OPr^i)_{16}$ was synthesised by hydrolysis of $Ti(OPr^i)_4$ with 1 equiv of water in i-PrOH solution at 100 °C for 3 days [9]. $Zr_{13}O_8(OCH_3)_{36}$ was synthesized by mixing dilute methanol solution of NaOH and the alkoxide of zirconium [10]. Bimetallic oligomeric structures are also possible: $Ba_4Ti_{13}O_{18}(OCH_2CH_2OCH_3)_{24}$ was synthesised by hydrolysis of barium titanium methoxyethoxide [11]. Oxo-alkoxide complexes $Ti_7O_4(OEt)_{20}$ and $Nb_8O_{10}(OEt)_{20}$ were obtained as single crystals by spontaneous decomposition upon prolonged storage or heating of solution of $Ti(OEt)_4$ and $NbO(OEt)_3$ [12], while $Ce_4O(OPr^i)_{14}$ was obtained by refluxing $Ce_2(OPr^i)_8(Pr^iOH)_2$ in toluene for 1.5 h [13].

Clustering of the Zr species in zirconium-rich PZT has been shown to affect the crystallization to the ferroelectric product, specifically, the formation of the transitory pyrochlore-type phase [14, 6].

In this context, we focused on PZ, the end-member of the PZT solid solution. In a previous paper [15] we studied the effect of hydrolysis conditions, namely pH and the water/Zr molar ratio R_w, on the decomposition pathway, crystallization and morphology of PZ dried powders. In the precursor, prepared with $R_w = 2$, where a dense gel structure was obtained, the organics decomposed with intermediate carbonaceous residues creating a reducing atmosphere in which Pb^{2+} was partially reduced to metallic Pb. The porous structure obtained at $R_w = 15$ facilitated the oxidation of the organic groups without any segregation of lead.

In the present paper we use extended x-ray absorption fine structure (EXAFS) for studying the local environment of metallic species of PZ precursor sol, dried and heated powder prepared with different hydrolysis conditions in order to determine their evolution along the synthesis path, with special emphasis to its early stage prior to hydrolysis.

2 Experimental Section

2.1 Synthesis

PZ was prepared from lead acetate and zirconium butoxide in *n*-butanol. The synthesis conditions have been described elsewhere [15]. The hydrolysis of the sol, PZ-L (L = liquid), was performed using a molar ratio of $H_2O/Zr(OC_4H_9)_4$ R_w = 2, 5 and 15 in neutral medium, and the resultant powders were denoted PZ(R_w)-D, and $R_w = 15$ in alkaline medium, denoted as 11PZ-D (D = dried). The molar ratio of $Zr(OC_4H_9)_4$:NH_3 (aq.) was 1:5. The hydrolysis products were dried to powder at 150 °C/12 h. The 11PZ-H (H = heated) powder resulted by heating the 11PZ-D powder, at 400 °C/1 h. In this paper, when referring to a specific sample the name of the sample is used, while for the dried powders as a group PZ-D is preferred.

2.2 EXAFS measurements, sample preparation and analysis

The absorption spectra were measured at XAFS (BL 11.1) beamline of ELETTRA synchrotron radiation facility in a standard transmission mode at room temperature. The ELETTRA storage ring operated in multibunch mode at electron energy of 2.4 GeV and a current of about 140 mA. A Si(111) double crystal monochromator was used with 1 eV resolution at the Pb L3-edge (13,035 eV) and 1.5 eV resolutions at the Zr K-edge (17,998 eV).

The intensity of the incident and transmitted monochromatic x-ray beam was measured by three consecutive ionization chambers. The first one was filled with 110 mbar of Ar and 1,890 mbar of N_2, the second with 800 mbar of Ar and 1,200 mbar of N_2 and the third with 2,000 mbar of Ar in case of Pb EXAFS experiments, while for Zr-K edge EXAFS the first was filled with 300 mbar of Ar and 1,700 mbar of N_2, the second with 2,000 mbar of Ar, and the third with 400 mbar of Kr and 1,600 mbar of N_2. Some of absorption spectra at Pb L_3-edge and Zr K-edge on powdered samples were measured also at X1 station in HASYLAB at DESY (Hamburg, Germany) in a standard transmission mode at room temperature. A Si(311) double-crystal monochromator was used with 2 eV resolutions at 18 keV. Harmonics were effectively eliminated by detuning the monochromator crystal using a stabilization feedback control. The three ionisation cells (first, second and third) were filled with 400 mbar Ar, 1,000 mbar Kr and 1,000 mbar Kr, respectively for Pb EXAFS experiments, while for Zr EXAFS measurements the first was filled with 1,000 mbar Ar and the other two with 1,000 mbar Kr.

The absorption spectra were measured within the interval [−250 eV to 1,000 eV] relative to the respective edge. In the XANES region equidistant energy steps of 0.5 eV were used, while for the EXAFS region equidistant energy steps of 2 eV were adopted with the integration time of 2 s/step. With several consecutive runs of each spectrum, the signal-to-noise ratio was improved. Exact energy calibration was established with simultaneous absorption measurements on a 10 μm thick Pb or Zr metal foil placed between the second and the third ionization chamber in all experiments. Absolute energy reproducibility of the measured spectra was ±0.1 eV or better.

The XAFS measurements were performed on liquid and powdered samples. The sol (liquid) sample (0.5 M solution) was prepared in inert atmosphere and sealed in a thin vacuum-tight plastic bag to prevent hydrolysis in air. The powdered samples were prepared in the form of homogeneous pellet; the sample material in the form of fine powder (20 mg/cm^2) was mixed with boron nitride (100 mg/cm^2) powder and pressed into self-supported pellets. In all cases

the samples with optimum absorption thickness of about 2 above the investigated absorption edge were prepared and inserted in the monochromatic beam between the first and second ionization cells. Exact energy calibration was established with simultaneous absorption measurements on a 10 micron thick Pb or Zr metal foil placed between the second and the third ionization chamber in all experiments. Absolute energy reproducibility of the measured spectra was ±0.1 eV or better.

The quantitative analysis of EXAFS spectra was performed with the IFEFFIT program packages [16]. Structural parameters were quantitatively resolved by comparing the measured signals with model signals, constructed ab initio with the FEFF6 program code [17] from the set of scattering paths of the photoelectron in a tentative spatial distribution of neighbour atoms. In the process, the atomic species of a neighbour was recognized by its specific scattering factor and phase shift. The least-square determination of structure parameters was performed in k-range = 4–12 $Å^{-1}$ for Zr K-edge and 4.3–13 $Å^{-1}$ for Pb L_3-edge. The amplitude reduction factor (S_o^2) was fixed to 0.9 for both edges. The least-square fits of the PZ-D spectra were performed at both edges simultaneously, so that the parameters of the path linking Pb and Zr atoms could be restrained to the same values in both spectra. The coordination numbers and corresponding Debye–Waller factors are strongly correlated. To avoid large error brackets arising in the correlation the Debye–Waller factors were kept fixed at a common average value.

3 Results

3.1 Pb-L_3 edge

Figure 1 presents Pb-L_3 edge EXAFS spectra of all samples. Prominent peaks in the Fourier transforms of the EXAFS spectra are the fingerprints of the photoelectron backscattering on the near neighbours around Pb atom. FT EXAFS spectra can be regarded as an (approximate) radial distribution of the neighbours, taking into account a systematic downward shift of the peaks due to photoelectron wave dispersion. Qualitative comparison indicates that the structure of the immediate neighbourhood at about 2 Å is retained, while significant changes are observed in the second coordination shell at about 3.5 Å. The intensity of the second peak in the spectrum of PZ-L sample is reduced to about half the value in the spectra of PZ-D samples, and is completely absent in the spectrum of 11PZ-H sample.

The local environment of Pb atoms can be reliably deduced in the quantitative EXAFS analysis, performed in the k interval from 4.3 Å to 13 Å. The complete list of the best fits structural parameters is collected in Table 1. The

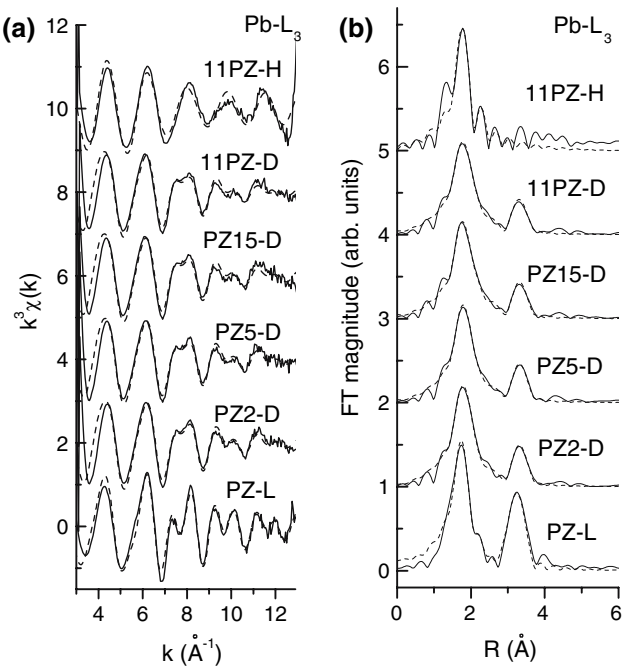

Fig. 1 k^3 weighted Pb-L_3 data (**a**) and their k^3 weighted Fourier transforms (**b**) of PZ sol, PZ dried powders prepared with different hydrolysis conditions and 11PZ powder heated at 400 °C/1 h. Solid line—experiment, dashed line—EXAFS model

Pb atom is coordinated to two O atoms: one at 2.22 Å, one at 2.37 Å in all samples. This large splitting of the oxygen shell is statistically validated with regard to a single distance shell, with a significant decrease in the relative chi-square value.

In the second coordination shell, we found two Zr atoms at nonequal distances in PZ-L: one at 3.45 Å and one at 3.58 Å. In the spectra of PZ-D powders only one Zr neighbour is present, located at the distance of 3.58 Å. After heating at 400 °C (11PZ-H sample) the Pb–O–Zr correlation is lost: there are no Zr neighbour atoms in the second coordination sphere of Pb.

3.2 Zr-K edge

Zr-K edge EXAFS spectra of all the samples are presented in Fig. 2. Fourier transforms of the EXAFS spectra all samples exhibit two prominent peaks. The quantitative EXAFS analysis, performed in the *k* interval from 4 $Å^{-1}$ to 12 $Å^{-1}$, reveals that the first peak in all spectra is contributed by the nearest coordination shell of O atoms distributed between 2.10 Å and 2.25 Å. At larger distances C, Zr and Pb neighbours are identified in all cases except for 11PZ-H sample, where Pb is not present. The best fit parameters of the nearest coordination shells around Zr atoms are collected in Table 2.

Table 1 Parameters of the nearest coordination shells around Pb atoms in PZ samples

Sample	Scattering atom	N	R(Å)	σ^2	R-factor
PZ-L	O	1.4(1)	2.21(1)	0.006	0.015
	O	0.7(1)	2.37(2)		
	Zr	0.6(1)	3.45(2)	0.006	
	Zr	1.2(1)	3.58(1)		
PZ2-D	O	1.0(1)	2.20(2)	0.005	0.005
	O	0.8(1)	2.33(2)		
	Zr	1.0(1)	3.58(2)	0.012	
PZ5-D	O	1.0(1)	2.21(1)	0.005	0.004
	O	0.7(1)	2.35(2)		
	Zr	1.0(1)	3.58(2)	0.012	
PZ15-D	O	1.0(1)	2.21(1)	0.005	0.005
	O	0.8(1)	2.35(2)		
	Zr	1.0(1)	3.59(2)	0.012	
11PZ-D	O	1.0(1)	2.21(2)	0.005	0.005
	O	0.8(1)	2.34(3)		
	Zr	1.0(2)	3.58(3)	0.014	
11PZ-H	O	1.2(1)	2.22(1)	0.004	0.032
	O	0.6(2)	2.39(2)		

Type of neighbour atom, their average number *N*, distances R and Debye–Waller factors σ^2 are listed. Uncertainty of the last digit is given in parenthesis. For parameters that are kept fixed in the fit, the error brackets are omitted. The quality of the fit is indicated by R-factor [16]

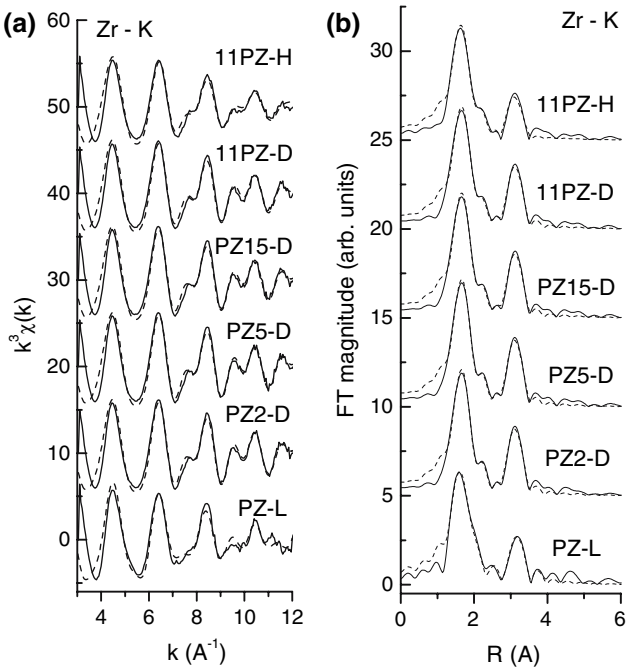

Fig. 2 k^3 weighted Zr-K data (**a**) and their k^3 weighted Fourier transforms (**b**) of PZ-L sol, PZ-D dried powders prepared with different hydrolysis conditions and 11PZ-H powder heated at 400 °C/1 h. Solid line—experiment, dashed line—EXAFS model

Table 2 Parameters of the nearest coordination shells around Zr atoms in PZ samples

Sample	Scattering atom	N	R(Å)	σ^2	R-factor
PZ-L	O	4.3(5)	2.10(1)	0.003	0.014
	O	3.4(5)	2.25(1)		
	C	1.35 ± 1.4	2.61(6)	0.007	
	Zr	6.4 ± 1.1	3.49(1)	0.013	
	Pb-set	0.6(1)	3.45(2)	0.006	
	Pb-set	1.2(1)	3.58(1)		
PZ2-D	O	4.4(3)	2.12(1)	0.003	0.005
	O	2.5(2)	2.26(1)		
	C	1.4(8)	2.73(3)	0.008	
	Zr	4.9(3)	3.46(1)	0.009	
	Pb	1.0(1)	3.58(2)	0.012	
PZ5-D	O	4.3(3)	2.12(1)	0.003	0.004
	O	2.5(2)	2.25(1)		
	C	1.3(7)	2.73(3)	0.008	
	Zr	4.8(3)	3.45(1)	0.009	
	Pb	1.0(1)	3.58(2)	0.012	
PZ15-D	O	4.3(3)	2.11(1)	0.003	0.005
	O	2.7(2)	2.25(1)		
	C	1.3(8)	2.74(3)	0.008	
	Zr	4.6(3)	3.46(1)	0.009	
	Pb	0.9(1)	3.59(2)	0.012	
11PZ-D	O	4.3(3)	2.11(1)	0.003	0.005
	O	2.7(2)	2.25(3)		
	C	1.2(7)	2.73(4)	0.008	
	Zr	4.9(3)	3.46(1)	0.010	
	Pb	1.0(2)	3.58(3)	0.014	
11PZ-H	O	4.3(4)	2.11(1)	0.003	0.010
	O	2.5(4)	2.25(3)		
	C	1.0(9)	2.72(4)	0.007	
	Zr	4.9(8)	3.44(1)	0.013	

Type of neighbour atom, their average number *N*, distances R and Debye–Waller factors σ^2 are listed. Uncertainty is given as a full number or in parenthesis where the case of the last digit. For parameters that are kept fixed in the fit, the error brackets are omitted. The quality of the fit is indicated by R-factor [16]

In PZ-D spectra the number of O neighbours is diminished from about eight to about seven, number of Zr neighbours is diminished from six to five and number of lead neighbours is diminished from two to one. After heating at 400 °C (11PZ-H sample) the structure of Zr local neighbourhood is retained, except that there are no Pb neighbours, in agreement with Pb L3 edge EXAFS results.

4 Discussion

In the synthesis of PZ, zirconium butoxide and lead acetate come in contact through the mediation of the solvent,

n-butanol. Peter et al. [18] investigated zirconium *n*-butoxide diluted in the parent alcohol. Their analysis revealed that zirconium *n*-butoxide adopted a dimer configuration, where Zr is 6-fold coordinated. The lead acetate does not dissolve in *n*-butanol and a clear sol is obtained by the reactive dissolution of lead acetate in zirconium butoxide in butanol with butyl-acetate elimination or addition reaction [19, 20, 21]. Pb–Zr correlations are explained through these reactions.

The higher coordination number of Zr (about eight) and relatively large number of Zr–Zr correlations (about six) that we found in the PZ-L may be explained by the ether elimination during thermolysis [12] (Eq. 1),

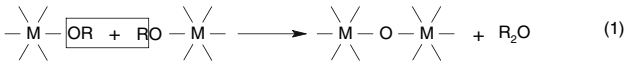

(1)

where M = Zr in the present work.

We propose that polynuclear oxo-alkoxide complexes form during reflux and distillation as has been reported for Ti, Nb and Ce alkoxides [12, 13]. The ether to form in our case is butyl-ether, boiling point = 142 °C, which forms an azeotrope mixture with *n*-butanol at the molar fraction 0.13:0.87 and b.p. = 117.4 °C, which is 0.3 °C lower than the b.p. of *n*-butanol. The butyl-acetate also forms an azeotrope mixture with *n*-butanol with molar fraction 0.23:0.77 and boiling point = 116.8 °C [22]. Both azeotrope mixtures are removed as by-products of distillation.

The links between Pb and Zr atoms are established by reactive dissolution of lead acetate in zirconium *n*-butoxide in butanol upon heating. By EXAFS analysis, we found that Zr atoms are building oxo-alkoxides complexes and Pb atoms are connected to Zr atoms. We propose that the links Pb–O–Zr are formed prior to the formation of Zr oxo-alkoxide complexes.

The next step of the synthesis is hydrolysis, where alkoxide groups are exchanged with hydroxyl groups (Eq. 2). The resulting species are very reactive and immediately undergo a condensation reaction (Eq. 3) with the formation of M–O–M bridges [2]:

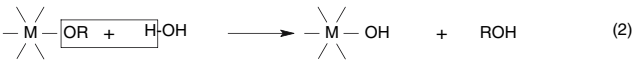

(2)

(3)

The analysis of the PZ-D samples shows that only the Pb–O–Zr link at 3.58 Å persists after the hydrolysis and drying, while the link at 3.45 Å is completely lost. The Zr coordination number decreased from eight to seven and Zr–O–Zr links diminished from six to five. Under all the hydrolysis conditions, similar products are formed and only one Pb–O–Zr link persists after hydrolysis and drying which means that the Pb atoms are still a component part of the Zr hydrolyzed product.

The analysis of the powder 11PZ-H shows that Pb is surrounded by two O atoms only (Table 1). The local environment of Zr (Table 2) is very similar to that of the PZ-D powders, the coordination number and the number of Zr neighbours is the same as in the PZ-D powders with the exception of the link with Pb. To sum up, the Pb–O–Zr links are completely lost.

The Pb–O–Zr links, achieved during the sol synthesis, are gradually lost, while Zr–O–Zr links remain stable from the sol to the powder heated at 400 °C.

5 Conclusions

PZ have been prepared by an alkoxide-based sol–gel route. The precursor solution synthesized from lead acetate, zirconium *n*-butoxide and *n*-butanol as solvent is hydrolysed in neutral and alkaline medium with different amounts of water.

In the sol, the lead environment is dominated by two Pb–O–Zr links, while the initial dimeric structure of Zr *n*-butoxide transforms during thermolysis to Zr oxo-alkoxide complex, where the Zr environment is populated by six Zr–O–Zr links.

After hydrolysis of the sol, one of the two Pb–O–Zr links is lost while Zr–Zr correlations are retained for a wide range of the Rw values. In the heated powder the Pb–Zr correlation is completely lost, while the Zr–Zr correlations remain almost unchanged. In contrast to the prevailing belief, atomic homogeneity is not entirely lost in the process of hydrolysis and condensation. To regain the homogeneity during crystallization into the desired perovskite phase of the end product, both Pb and Zr environment have to suffer major changes.

Acknowledgements This work has been supported by the Slovenian Research Agency research programme P1-0112 and P2-105, by EU Centre of Excellence SICER (G1MA-CT-2002-04029), by DESY, ELETTRA and the European Community under the FP6 Programme "Structuring the European Research Area" contract RII3-CT-2004-506008 (IA-SFS). Access to synchrotron radiation facilities of ELETTRA (beamline XAFS, project 2006114) and HASYLAB (beamline E4, project II-04-065) is acknowledged. We would like to thank Luca Olivi of ELETTRA and Edmund Welter of HASYLAB for expert advice on beamline operation and to Jana Padeznik Gomilsek for help in XAFS measurements.

References

1. Jaffe B, Cook WR Jr, Jaffe H (1971) Piezoelectric Ceramics. Academic Press Inc. London Ltd

2. Brinker CJ, Scherer GW (1990) Sol-gel science, the physics and chemistry of sol-gel processing. Academic Press, New York
3. Lakeman CDE, Xu Z, Payne DA (1995) J Mater Res 8:2042
4. Sengupta SS, Ma L, Alder DL, Payne DA (1995) J Mater Res 10(6):1345–1348
5. Feth MP, Weber A, Merkle R, Reinohl U, Bertagnolli H (2003) J Sol-Gel Sci Tech 27:193–204
6. Malic B, Arcon I, Kodre A, Kosec M (1999) J Sol-Gel Sci Tech 16:135–141
7. Malic B, Kosec M, Arcon I, Kodre A (2005) J Eur Cer Soc 25:2241–2246
8. Malic B, Arcon I, Kodre A, Kosec M (2006) J App Physics 100:051612
9. Day VW, Eberspacher TA, Klemperer WG, Park CW (1993) J Am Chem Soc 115:8469–8410
10. Morosin B (1977) Acta Cryst B33:303–305
11. Campion J-F, Payne DA, Chae HK, Maurin JK, Wilson SR (1991) Inorg Chem 30:3244–3245
12. Turova NY, Turevskaya EP, Kessler VG, Yanovskaya MI (2002) The chemistry of metal alkoxides. Kluwer Academic, Boston
13. Sirio C, Hubert-Pfalzgraf LG, Bois C (1997) Polyhedron 7: 1129–1136
14. Polli AD, Lange FF, Levi CG (2000) J Am Ceram Soc 83: 873–881
15. Ion ED, Malic B, Kosec M (2007) J Eur Cer Soc 27:13–15
16. Ravel B, Newville M (2005) J Synchrotron Rad 12:537–541
17. Rehr JJ, Albers RC, Zabinsky SI (1992) Phys Rev Lett 69: 3397–3400
18. Peter D, Ertel TS, Bertagnolli H (1994) J Sol-Gel Sci Tech 3:91–99
19. Kosec M, Malic B (1995) Forth Euro Ceramics 5:9–16
20. Malic B, Arcon I, Kosec M, Kodre A (1997) J Sol-Gel Sci Tech 8:343–346
21. Malic B, Kosec M (2002) MIDEM 32(4):231–237
22. Gmehling J, Menke J, Krafczyk J, Fischer K, Fontaine J-C, Kehiaian HV (2006–2007) CRC handbook of chemistry and physics, 87th edn. 6:155–173